Atmospheric Environment 201 (2019) 334–347

Contents lists available at ScienceDirect

Atmospheric Environment

journal homepage: www.elsevier.com/locate/atmosenv

Air quality trends of the Kathmandu Valley: A satellite, observation and modeling perspective

Parth Sarathi Mahapatra[a,*], Siva Praveen Puppala[a,*], Bhupesh Adhikary[a], Kundan L. Shrestha[b], Durga Prasad Dawadi[c], Shankar Prasad Paudel[c], Arnico K. Panday[a]

[a] International Centre for Integrated Mountain Development (ICIMOD), G.P.O. Box 3226, Kathmandu, Nepal
[b] Department of Environmental Science and Engineering, Kathmandu University, Dhulikhel, Kavre, Nepal
[c] Department of Environment (DoEnv), Ministry of Population and Environment, Kathmandu, Nepal

ARTICLE INFO

Keywords:
Aerosol optical depth
South Asia
Air quality
Weather research and forecasting
Cities
Nepal

ABSTRACT

Kathmandu is the capital city of Nepal and a 'hotspot' of urban air pollution in South Asia. Its bowl-shaped structure (altitude 1300 m above sea level (masl); floor area 340 km^2) surrounded by tall mountains provides a unique case study for analyzing pollution trapped by topography and local meteorology. In the absence of long-term in-situ observations, for the first time the columnar aerosol loading trend of the Kathmandu Valley was analyzed using satellite-derived aerosol optical depths (AOD). AOD from MODIS (Moderate Resolution Imaging Spectroradiometer) onboard Aqua and Terra (3 × 3 km, Level 2) was used during the dry season (November–June) in 2000–2015. Trend analysis of Kathmandu AOD (K_{AOD}) (the Kathmandu Valley AOD ($KVal_{AOD}$) + background AOD (B_{AOD})) suggested an increase of ~35% during the study period. To derive the $KVal_{AOD}$ trend, B_{AOD} was subtracted from K_{AOD}. The $KVal_{AOD}$ trend indicated an increase of ~50–60% during the study period, based on MODIS Aqua and Terra data. Thereafter, the background contribution only at the valley layer (1300–1400 masl) was determined using Cloud-Aerosol LiDAR and Infrared Pathfinder Satellite Observation (CALIPSO) profiles, in-situ observation and modeling techniques. The CALIPSO-based analysis indicated that background pollution contributed an additional 20–25% to local pollution. This finding was further supported by short-term in-situ measurements from Dhulikhel (the site where Kathmandu background measurements were taken) and Ratnapark (a Kathmandu city center site). Case studies were conducted using chemical transport models (WRF-STEM and WRF-Chem) to quantify the contribution of background air pollution to the Kathmandu valley pollution. These model results contradicted the satellite and in-situ observation by highly underestimating the Kathmandu Valley pollution levels. Comparison of visibility in Kathmandu with AOD suggests a profound role of B_{AOD} on decreasing long-distance visibility in particular months.

1. Introduction

Urban air pollution has become a global problem with distinct effects in the world's developing cities. This situation becomes more noticeable in cities located within a basin and surrounded by mountains. Mountains act as a natural barrier to horizontal winds that usually blow away the locally emitted pollutants. The result of this is that dispersal of pollutants within a valley (Kathmandu in this case) becomes strongly dependent on the orientation of mountain passes, wind circulation and local meteorology prevalent within the valley. Specifically, at night the mountain slopes become increasingly cold, pushing the heavier air mass which settles down, suppressing the vertical mixing of air masses. During the day, the heating of slopes helps pollutant transport, but this is highly dependent on the orientation of mountain passes within the valley and the topography of the mountains outside it (Panday et al., 2009).

Rapidly urbanizing cities located in the developing region and with similar complex topography are vulnerable to challenges presented by changes in the local air quality. In the recent past, several cities with complex topography and meteorology, such as Mexico and Santiago de Chile, have been studied extensively (Cakmak et al., 2007; Gómez-Arroyo et al., 2017; Molina et al., 2007; Romero et al., 1999). However, other cities with similar features in developing countries and global hotspots have been less studied. In this context Kathmandu Valley, the largest metropolitan region in Nepal and with a complex topography-cum-meteorology, serves as a good case study in the South Asian region

* Corresponding authors.
E-mail addresses: parth.mahapatra@icimod.org (P.S. Mahapatra), SivaPraveen.Puppala@icimod.org (S.P. Puppala).

https://doi.org/10.1016/j.atmosenv.2018.12.043
Received 25 May 2018; Received in revised form 18 December 2018; Accepted 30 December 2018
Available online 11 January 2019
1352-2310/

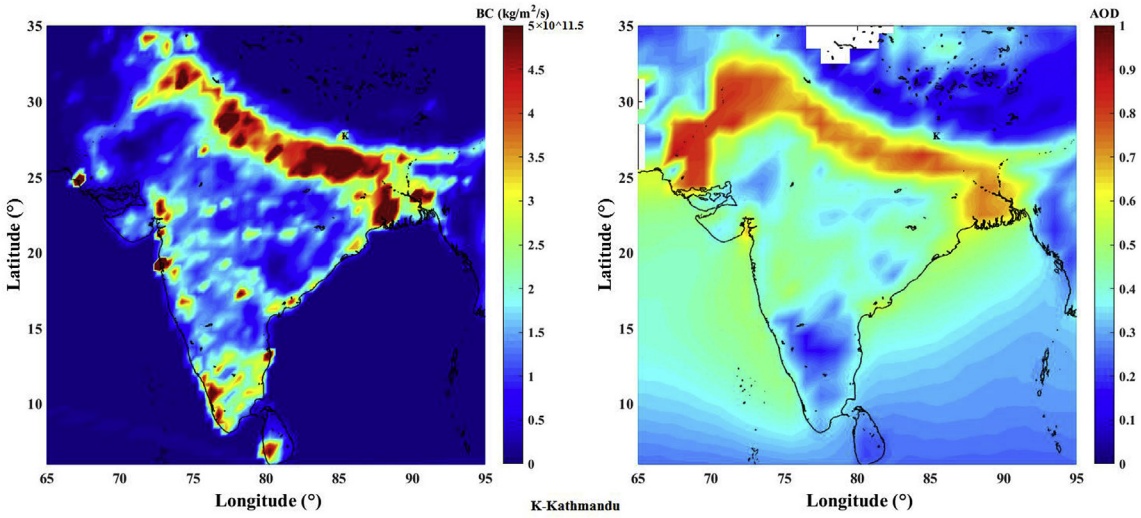

Fig. 1. Left panel: spatial distribution of black carbon from RCP emissions inventory averaged over 2005 and at a resolution of 0.5° × 0.5°. Right panel: spatial distribution of AOD from MODIS averaged for the years 2000–2015 at a resolution of 1° × 1°. The letter 'K' denotes location of the Kathmandu Valley. The areas with increasingly red color denote regions with higher concentration of aerosols. (For interpretation of the references to colour in this figure legend, the reader is referred to the Web version of this article.)

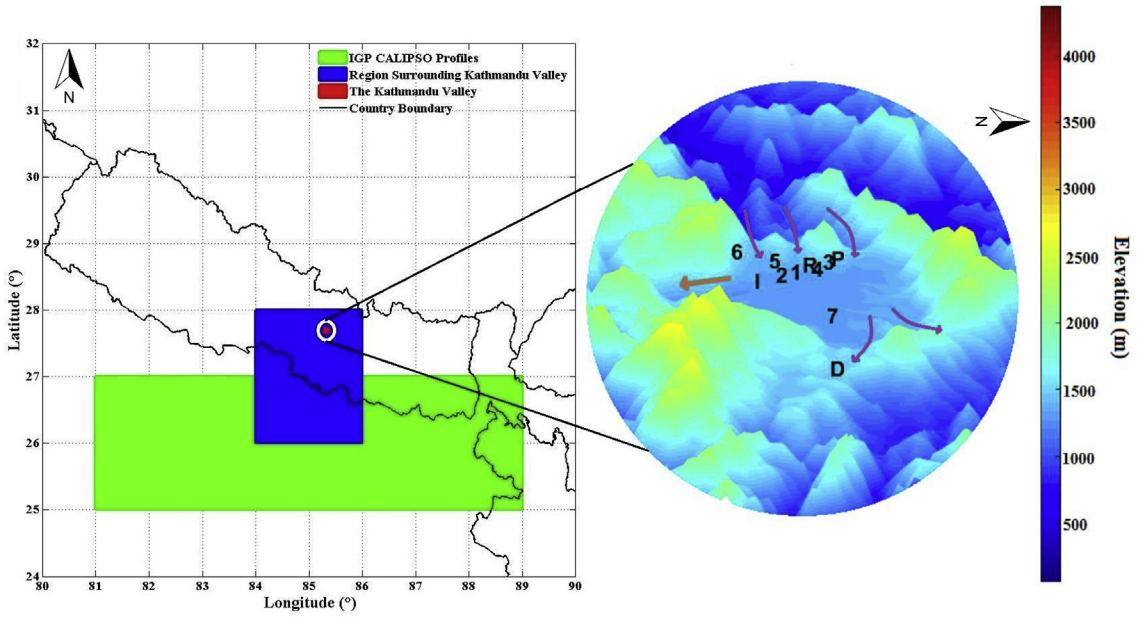

Fig. 2. Left panel: site map of the Kathmandu Valley, Nepal, and surrounding locations used to generate the different satellite data presented in the study. Right panel: magnified map of Kathmandu Valley and its topography. The various measurement sites indicated in the literature are: 1, Pulchowk College Monitoring Site; 2, Patan Hospital; 3, Thamel; 4, Putalisadak; 5, Tribhuvan University; 6, Matsyagaon; 7, Bhaktapur; P-Paknajole; I-ICIMOD; R- Ratnapark and D-Dulikhel, are shown in Fig. 2. Sites 2–7 represent sites of government air quality monitoring. The five mountain passes surrounding the valley are shown in purple arrows and one river outflow in brown arrow. (For interpretation of the references to colour in this figure legend, the reader is referred to the Web version of this article.)

(Fig. 1, letter 'K'; Fig. 2, red grid). Regionally, the Kathmandu Valley is located in the mid-hills of Nepal, with the Indo-Gangetic Plains (IGP) in the south and Tibet in the north (Fig. 1). The IGP are a densely populated area and well known for high levels of air pollution. The high pollution loading can be distinctly observed in a time-averaged RCP (Representative Concentration Pathways) emission inventory map for anthropogenic black carbon (BC) (van Vuuren et al., 2011, 2007) and MODIS v.6, AOD maps (Fig. 1). The RCP emission inventory map was averaged over 2005 and at a resolution of 0.5° × 0.5°, while the AOD map was averaged for the years 2000–2015 at a resolution of 1° × 1°. This region is characterized by a mixture of emissions including biomass burning (due to biomass used for cooking, and outdoor burning activities in large rural areas, seasonal forest fires), and emissions from vehicles and coal-based thermal power plants and industries (Lawrence and Lelieveld, 2010; Rupakheti et al., 2017; Saud et al., 2012; Sharma et al., 2016; Tiwari, 2013). With an air pollution-rich region (the IGP) situated south of the Kathmandu Valley and at a lower elevation, a certain amount of pollution is anticipated to reach Kathmandu through long-range transport/advection processes (Bhardwaj et al., 2017; Putero et al., 2015). Most studies characterizing the air quality within the valley indicate the presence of some pollution coming from outside Kathmandu (background pollution indicating sources other than Kathmandu), but have not been successful in quantifying the same.

Apart from the topography of Kathmandu and background pollution, the air quality problem is aggravated by rapid population growth, a subsequent increase in energy demands and unplanned developments.

The human population within the Kathmandu Valley grew from 16,45,091 to 25,17,023 during 2001–2011 (Central Bureau of Statistics Nepal, 2012; Central Bureau of Statistics of Nepal - Economic Demography, 2014). Consequently, the valley has observed unprecedented growth in vehicular fleets, which increased rapidly at a rate of ~14% per year during 2000–2010 (Shrestha et al., 2013). The total energy consumption of the Kathmandu Valley is estimated to increase at an average annual growth rate (AAGR) of 3.2% for the period 2005–2050 (Shrestha and Rajbhandari, 2010). Local newspapers and magazines write about 'air quality, worsening continuously' or reduced visibility challenges, but precise statistics to support the claim are not yet available. The present study used an integrated approach, with satellite data, observation and modeling tools to address these issues.

Broadly, the study divides into three sections: (1) addressing the changes in columnar aerosol trend within the Kathmandu Valley in the past 15 years (2000–2015) using satellite-derived AOD; (2) estimating the contribution of background pollution at the Kathmandu Valley layer (1300–1400 m) using CALIPSO data, observation and models; and (3) explaining urban air quality issues, visibility and the role of Kathmandu pollution or the background pollution influencing it.

2. Site description

Fig. 2 shows the location of Kathmandu, Nepal, in the left panel. The right panel shows a magnified map of the Kathmandu Valley with topographical features. The numbers and letters in the figure denote the sites where earlier measurements were carried out. The Kathmandu Valley is a broad, flat, basin-shaped structure with an approximate floor area of 340 km^2 situated at a mean elevation of ~1300 m above sea level (masl) located in the central region of Nepal (Panday and Prinn, 2009). It is surrounded by a ring of tall mountains with elevations ranging between 2000 m and 2800 m, making a complex topography around the valley (Fig. 2, right panel). The valley has five mountain passes (Nagdhunga, Bhimdhunga, Mudkhu Bhanjyang, Sanga and Nagarkot) at an approximate height of 1500–1550 masl in the northwestern and southeastern sectors, which serve as major pathways for air pollutants to enter or leave (Fig. 2, right panel). On winter mornings, in particular, the combination of suppressed mixing, katabatic wind flow and basin topography cause pollutants to remain trapped under an inversion layer close to the valley base (Kitada and Regmi, 2003; Panday and Prinn, 2009). This provides a unique case for studying pollution trapped by topography and meteorology. The South Asian summer monsoon drives the changes in seasons for the Kathmandu Valley. It receives 90% of its annual rainfall during 3–4 months, and is dry for the remainder of the year.

3. Past research in the Kathmandu Valley region

Early measurements of air quality in the Kathmandu Valley date back to the 1980s when few air quality parameters (sulfur dioxide, SO_2; nitrous oxide, NO_2; carbon monoxide, CO; non-methane hydrocarbons, NMHCs) were measured, and then only in campaigns during different seasons. These studies provided some initial pollutant levels and shed light on the seasonality of air pollution in the valley (Davidson et al., 1986; Kitada and Regmi, 2003; Regmi and Kitada, 2003; Sharma et al., 2000).

Later, the government of Nepal also realized the importance of monitoring air quality and established six air quality monitoring stations at different locations in the valley for measuring PM (particulate matter) concentrations. Measurements of PM_{10} highlighted that urban residential and traffic sites were ~3–4 times more polluted than the background sites present in the valley (Table 1) (Aryal et al., 2009, 2008; Giri et al., 2006; Gurung and Bell, 2012; Panday et al., 2009). $PM_{2.5}$ concentrations from two different studies conducted during 2006–2007 suggested that urban residential sites (Thamel) (Aryal et al., 2009) were ~2.5 times more polluted than a background location (Godavari) (Stone et al., 2010). These studies indicated that the valley itself was highly polluted and that background sites were less polluted. Unfortunately, these measurements continued for only a short period (2002–2007), or were made in campaign modes, and thus did not reveal any long-term patterns.

As interest in understanding the air quality in the Kathmandu Valley increased, for the first time BC aerosol mass concentrations were measured in 'Pulchowk', an urban site in the Kathmandu Valley, from May 2009 to April 2010 (Sharma et al., 2012). This was followed by measurements at ICIMOD (a semi-urban site close to the valley edges) from December 2012 to January 2013, and at Paknajole (an urban site in the city center) from February 2013 to January 2014. Thereafter several large scale, multi-country collaboration based campaigns ('SusKat' and 'NAMaSTE') were conducted to understand the different air quality related issues in Nepal (Bhardwaj et al., 2017; Jayarathne et al., 2018; Kim et al., 2015; Mahata et al., 2018; Rupakheti et al., 2017; Sarkar et al., 2017; Shakya et al., 2017; Shrestha et al., 2017; Stockwell et al., 2016). Results from these studies indicate that pollutant concentrations were much higher in the valley center than in its periphery. However, a large gap still exists in understanding the long-term trend of air pollution, and stronger evidence on the contribution of background pollution to Kathmandu Valley pollution levels is needed.

4. Methodology

4.1. Satellite data

Aerosol optical parameters are some of the numerous products retrieved operationally from MODIS onboard the two Earth Observing System (EOS) satellites, Terra and Aqua. These are operated by the US National Aeronautics and Space Administration (NASA) and were launched on 18 December 1999 and 4 May 2002, respectively (operating altitude ~705 km). AOD is one of the aerosol optical parameters retrieved from MODIS. This is an optical measure of light extinction (absorption and scattering) of the solar beam due to the amount of total aerosols (dust, haze, particles) in the entire atmospheric column, and provides an indirect measure of aerosols in the atmosphere (He et al., 2017). MODIS has a high spatial resolution (up to 250 m at nadir), wide swath (2330 km, which gives it the capacity to monitor the entire world once daily) and large spectral range (36 channels between 0.412 μm and 14.2 μm, of which 29 spectral bands are at 1-km resolution, 5 are at 500-m resolution and 2 are at 250-m resolution, nadir pixel dimensions) (Levy et al., 2005). The Level-2 AOD (at 550 nm; swath 3 km) data product (MOD04_3K/MYD04_3K, based on the standard dark target retrieval algorithm) used in this study was downloaded using the LAADS (Level 1 and Atmospheres Archive and Distribution System) online data acquisition portal (https://ladsweb.nascom.nasa.gov/) without applying any corrections. For the present study, AOD from MODIS Terra and Aqua were used for the period 2000–2015 and 2002–2015, respectively (Levy et al., 2013). Typically on a particular day, the number of AOD data points within the valley ranged from 1 to 9. A minimum of 3 AOD data points or above were observed in at least 60 percent of the days from both Terra and Aqua. A frequency distribution plot of the data points per day for the entire study period has been shown in Fig. S1. All AOD data points on a typical day were averaged on a daily basis and then analyzed on a monthly and annual basis. The AOD data used in our study have been validated by various studies (Gupta et al., 2018; He et al., 2017; Kumar et al., 2018; Livingston et al., 2014; Mhawish et al., 2017) in different parts of the world, including high-altitude locations framing a strong base to utilize these values for studying the Kathmandu Valley in the present case. AOD 3 km data product depends on the Land use Land cover (LULC) of the area of interest. Thus, changes in LULC within that 3 km might strongly affect the AOD values. Immediate changes in the topography of the area of interest would also affect the AOD values. However, within the known limitations, of the available data, this is the best way to

Table 1
Past studies of BC and PM in and around the Kathmandu Valley.

Sl. no.	Location lat./long.	Study period	BC μg/m^3	PM μg/m^3	Remarks	Study by
1.	Site 1	May 2009–Apr. 2010	8.4 ± 5.1		Annual	Sharma et al. (2012)
2.	Paknajol 27°43′4″ N, 85°18′32″ E 1380 m	Feb. 2013–Jan. 2014	11.6 ± 10.7	169 ± 113*	Annual	Putero et al. (2015)
3.	Site 'I' (ICIMOD)	Dec. 2011–Jan. 2013	6.6 ± 5.4		Annual	Personal communication
4.	Site 2	2003–2005		185.19 ± 72.91*	3 years mean	Giri et al. (2006)
	Site 3			133.71 ± 70.31*		
	Site 4			199.8 ± 86.18*		
	Site 5			69.91 ± 46.07*		
	Site 6			47.78 ± 32.28*		
	Site 7			104.01 ± 67.84*		
5.	Site 2	2003–2006		185.5 ± 77.25*	4 years mean	Aryal et al. (2008)
	Site 3			133.5 ± 71.25*		
	Site 4			210.75 ± 95.25*		
	Site 5			71.25 ± 44*		
	Site 6			48 ± 32.75*		
	Site 7			100.75 ± 68.75*		
6.	Thamel 27°42′21″ N 85°19′20″ E	2006–2007		~61 ± 22#	Pre-monsoon	Aryal et al. (2009)
7.	Godavari 27.59° N, 85.31° E, 1600 m	Year 2006		26 ± 19#	Annual	Stone et al. (2010)

*,PM_{10}; #, $PM_{2.5}$; Site 1, Pulchowk College Monitoring Site; Site 2, Patan Hospital; Site 3, Thamel; Site 4, Putalisadak; Site 5, Tribhuvan University (semi-urban); Site 6, Matsyagaon (valley background); Site 7, Bhaktapur (semi-urban); P-Paknajole and I-ICIMOD, are shown in Fig. 2. Sites 2–7 represent sites of government air quality monitoring.

understand the aerosol loading within the Kathmandu valley. The flat valley floor (340 km^2) of Kathmandu, with minimal variation in elevation and an almost urbanized land cover, is also expected to aid the satellites in capturing similar surface reflectance and generate enough AOD data points of good quality for studying the columnar aerosol loading within Kathmandu (discussed more in section 4.4.1). However, a certain level of limitations does persist with respect to the background AOD (B_{AOD}) calculation (discussed more in section 4.4.2) due to changes in the topography and LULC within the study domain. That being said, in order to overcome these shortcomings, we estimated the seasonal contribution of aerosol loading from the low lying plains using CALIPSO aerosol extinction profiles and AOD at different elevations (described in details in section 4.4.4). The background contribution obtained from these methods was compared with the B_{AOD} used in the study to determine their similarity. Hence, with the existing limitations, we also used different means to validate our logic of background calculation. Therefore, this was the best possible way to present the trend in aerosol loading over the Kathmandu valley as well as calculate the contribution of background air pollution to the valley. Furthermore, the daily average MODIS AOD for Aqua and Terra were compared with the daily average AERONET (AErosol RObotic NETwork) AOD for the available days (within the dry period, excluding the monsoon months) from 2012 to 2014 (Fig. S4). AERONET, Version 3, Level 2.0, AOD data at 500 nm was compared with Level-2 AOD (at 550 nm; swath 3 km) from MODIS for Aqua and Terra. Comparison of MODIS AOD and AERONET AOD indicated a small deflection in the slope (y = 0.88x for MODIS Aqua AOD vs AERONET AOD; y = 0.82x for MODIS Terra AOD vs AERONET AOD) with a moderate correlation (r^2 = 0.62 and 0.50). However, the slight variability in slope when compared to 1 might be due to the comparison of the daily average values for AERONET and MODIS, AOD. The slope of the correlation might get closer to 1 if only satellite overpass times were compared. Another study that validated MODIS 3 km AOD data product with different AERONET sites across the globe also reported similar values as that of the present study, providing strong basis for using MODIS 3 km data product. Overall, the comparison indicates a closer match between MODIS (AOD) and AERONET (AOD) providing enough confidence to use the MODIS AOD 3 km data product for studying the columnar aerosol loading over Kathmandu.

CALIPSO was developed as a partnership between NASA and the French Space Agency, CNES. It comprises three instruments, the Cloud-Aerosol LiDAR with Orthogonal Polarization (CALIOP LiDAR -a nadir-viewing two-wavelength, polarization-sensitive LiDAR), the Imaging Infrared Radiometer (IIR) and the Wide Field Camera (WFC) (IIR and WFC being passive sensors). CALIPSO was launched on April 28 2006 onboard A-Train (Afternoon Constellation) and flies in a 705 km sun-synchronous polar orbit providing global coverage between 82°N and 82°S. CALIOP provides measurements of the aerosol extinction profile at 532 and 1064 nm with a receiver field of view of 90 m and footprint spacing of 335 m. CALIPSO profiles for this study were downloaded for the period 2006–2014 (https://eosweb.larc.nasa.gov/HORDERBIN/HTML_Start.cgi) (Pistone et al., 2016; Qin et al., 2016).

4.2. Chemical transport model setup

Two regional-scale chemical transport weather research and forecasting (WRF) models (the Sulfur Transport and dEposition Model, WRF-STEM; and WRF coupled with chemistry, WRF-CHEM) were used to simulate the Kathmandu Valley pollution levels and the contribution from the background. Existing model outputs by two different modeling groups were used in the present study, only to support the results obtained from the satellite data analysis and in-situ measurements. Hence, generating model outputs for the exact same time was not possible for the study. However, the results of different time periods would also indicate if there are any changes in contribution of background air pollution to the Kathmandu valley pollution levels at different time periods. While different model set-ups were used to address issues if any associated with resolution (25 × 25 km in WRF-STEM vs 3 × 3 km in WRF-CHEM) and in-built feedback mechanisms (in WRF-CHEM there is a feedback mechanism between the chemistry and meteorology but in WRF-STEM it is absent). The WRF-STEM was run for a larger domain while that for WRF-CHEM was run for a smaller domain. The individual model set up have been discussed in the following sections 4.2.1 and 4.2.2.

4.2.1. WRF-STEM

In the present study, the WRF-STEM model was used to simulate the contribution of pollutants from within and outside the Kathmandu Valley. It uses region-tagged carbon monoxide (CO) tracers to identify the geographical contribution of pollutants (Adhikary et al., 2010). The model was simulated with fixed boundary conditions to link emissions

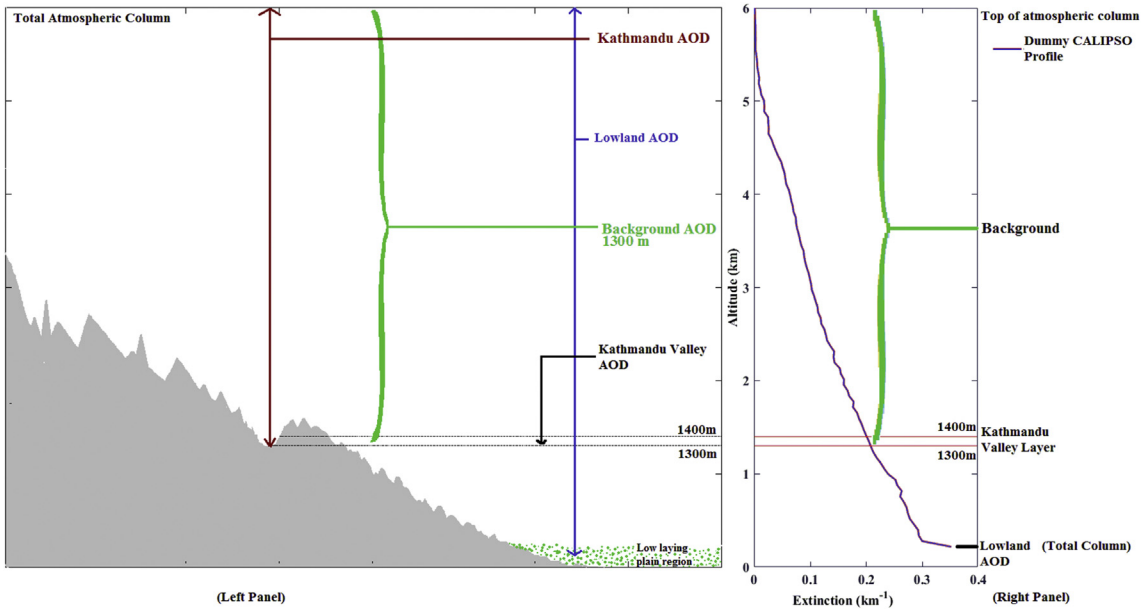

Fig. 3. Left panel: schematic representation of Kathmandu and different aerosol optical depth (AOD) terminologies used in the study (Kathmandu AOD, the Kathmandu Valley AOD, background AOD and lowland AOD). Right panel: A hypothetical CALIPSO profile indicating integrated aerosol extinction from the surface to the top of the column, to clarify the figure in the left panel.

with transport over a larger domain ranging from latitude 3.390–43.308° N and longitude 34.880 to 130.223°E and was centered at longitude 82.552° E and latitude 24.94° N. The model used a time step of 100 s with a horizontal grid resolution of 25 × 25 km, 425 grids in the east–west direction, 200 grids in the north–south along with 40 vertical layers with the top of the model set at 50 mbar. The WRF version 3.5.1 (Skamarock et al., 2008) was used to generate meteorological variables necessary as an input for the STEM to simulate the pollutants concentration. While the model was initialized using NCEP FNL (Final) data (ds083.2) with 1° × 1° resolution available from the University Corporation for Atmospheric Research (UCAR) website (http://rda.ucar.edu/datasets/ds083.2/). The anthropogenic emissions fed into the simulations were from HTAPv2 (available from http://edgar.jrc.ec.europa.eu/htap_v2/). More details regarding the model setup, simulations and its performance in the region can be seen in earlier research done by the group (Adhikary et al., 2007; Gul et al., 2018; Rupakheti et al., 2017). The model was given a 1-month spin-up period before the particular months used in this analysis (15 January – 15 February 2013 and 15 April – 15 May 2013 representing winter and summer season analysis), a standard practice when using this regional chemical transport model.

4.2.2. WRF-CHEM

WRF-Chem version 3.6.1 was used to simulate the air quality for the time period 1 April - 16 April 2015 and 1 November - 16 November 2015. The model used a Mercator projection and contained a single domain with horizontal spatial resolution of 3 km; the domain centered around Kathmandu Valley. The model used a time step of 20 s for 90 × 70 horizontal grids and 51 vertical levels. The initial and lateral meteorological boundary conditions were obtained from the NCEP FNL data set available for every 6 h at the spatial resolution of 1° × 1°. For the chemical boundary conditions, mozbc utility was used to incorporate the Model for Ozone and Related Chemical Tracers, version 4 (MOZART-4) data were used (Emmons et al., 2010). The anthropogenic emission was obtained from the Emission Database for Global Atmospheric Research (EDGAR HTAP V2) inventory (Janssens-Maenhout et al., 2012). The biogenic emission was obtained from the Model of Gases and Aerosols form the Nature (MEGAN 2.1) database (Guenther et al., 2012). For biomass burning data, the Fire Inventory from the National Center for Atmospheric Research (NCAR) (FINN) was used. In physics parametrization schemes, WSM 5-class scheme was the microphysics scheme, Grell 3D ensemble scheme was the cumulus parametrization, RRTM (Rapid Radiative Transfer Model) was the longwave radiation scheme, Dudhia scheme was the shortwave radiation, Unified Noah was the land surface model, and Yonsei University PBL (YSU) was the planetary boundary layer model. For chemistry parametrization, MOZART chemistry with Global Ozone Chemistry Aerosol Radiation and Transport (GOCART) aerosol (MOZCART) with Madronich F-TUV photolysis was used. The “mozbc” preprocessor tool, provided by the Atmospheric Chemistry Observations and Modeling Lab (ACOM) of NCAR at https://www2.acom.ucar.edu/wrf-chem/wrf-chem-tools-community was used to create chemical boundary conditions by mapping the MOZART-4 species to the WRF-Chem species. The WRF-Chem was also tested at other grid resolutions such as 6 km, 10 km and so on to see that use of the resolution of 3 km was suitable. In separate simulation experiments (not shown here), the results were validated with the ground data.

4.3. Statistical analysis

The plotting and calculations associated with this study were made using the MATLAB R2017a numerical computing environment from MathWorks, Inc. (www.mathworks.com). The IBMSPSS Statistics 20 software was used to run Kendall's tau-b test for determining the significance of trend analysis (Ross, 2017).

4.4. Concept of the study

AOD derived from MODIS provides an unparalleled option for estimating the changes in columnar atmospheric aerosol and hence the air quality on a regional scale (Vinoj et al., 2007). Analyzing changes in the AOD column over Kathmandu, therefore, provides an indirect measure of changes in the city's aerosol loading. Fig. 3 (left panel) provides a schematic representation of the Kathmandu Valley, its surrounding geography and different AOD terminologies used in this study. A hypothetical CALIPSO vertical aerosol extinction profile obtained over the low laying plain region, showing distribution of aerosols from the surface to the top of the column is shown in Fig. 3 (right panel). Because

AOD is a columnar product, the Kathmandu AOD (K_{AOD}) trend represents the changes in local aerosol loading due to sources in the valley (which roughly extends between 1300 m and 1400 masl) and additional sources from the background levels present in the valley. To derive the pollution trend from only the Kathmandu Valley sources, the AOD trend in the valley layer only (the Kathmandu Valley AOD, $KVal_{AOD}$, represented by the black and red lines in Fig. 3) has to be studied. To derive the AOD trend in the valley, we have to remove the background AOD (B_{AOD}) at 1300 m (represented by the green line in Fig. 3). Detailed description of the above discussed terminologies and their significance is continued in the following paragraphs.

4.4.1. Kathmandu AOD (K_{AOD})

Henceforth in the present study, K_{AOD} indicates the AOD points derived only in the core Kathmandu city area bounded by 85.281–85.371 E and 27.658–27.729 N. The region is demarcated by a red grid in the left panel of Fig. 2 and the brown line in Fig. 3. Data for AOD were derived on a daily basis throughout the study period. The data above mean $+3\sigma$ standard deviation was not considered for further analysis to remove AOD values that might be biased due to cloud cover. Hence, K_{AOD} represents pollutants integrated from within the valley ($KVal_{AOD}$) and background sources/B_{AOD} (Eqn (1)).

$$K_{AOD} = KVal_{AOD} + B_{AOD} \quad (1)$$

4.4.2. Background AOD (B_{AOD})

Geographically, Kathmandu is bounded by IGP in the South and Himalayas in the North. The nearest hot spot of air pollution is found South of Kathmandu in the IGP region. While in the North of Kathmandu lie the tallest mountains of the world which do not have any sources of air pollution. The statement is well-supported by the analysis presented for Fig. 1 (section 1). In the present study, there are no hot spots of air pollution around 1300 masl except the Kathmandu Valley. However, we can expect to see changes in AOD if there are any large scale forest fires or other significant sources of emissions. Hence, if we exclude, the Kathmandu valley region from the analysis, aerosol loading at 1300 masl elevation would represent the background levels of aerosol loading. Therefore, the same hypothesis has been applied in the present study to understand the contribution of background aerosol loading to the Kathmandu valley aerosol load. A hypothetical CALIPSO profile in the right panel of Fig. 3 shows the distribution of aerosol extinction from the surface to the top of the column. Over the low laying plain region, aerosol extinction above 1300 m may be representative of 'background' for mountain regions with elevations of 1300 m and above. The valley floor of Kathmandu city is situated at 1300 m elevation. Hence, advection from lowland AOD at 1300 m can be considered as 'background' for K_{AOD} (Fig. 3, right panel). Therefore, B_{AOD} was determined, considering the AOD at a similar height to the Kathmandu floor in nearby regions, but excluding Kathmandu, as Kathmandu is a source of pollution. The AOD at 1300 m height in a $2^\circ \times 2^\circ$ grid (latitude 26°–28° N and longitude 84°–86° E; blue grid in the left panel of Fig. 2) near to the Kathmandu Valley (but excluding it) was chosen as the B_{AOD}. All AOD points were georeferenced with latitude and longitude data. These geographical coordinates were then linked with a global digital elevation model (DEM) (Hastings and Dunbar, 1999), thereby deriving the height for those AOD points. The DEM used in the present study has a resolution of 1 km while that of AOD is 3 km. Due to the complex topography of the region, within short distances, the altitudes might also vary significantly. As a result of which minor errors is expected but any problem that might arise due to interpolation of the AOD and DEM data is not expected to hamper the quantitative findings of the study. As a long period of data set (15 years) has been used for analysis in the study. Also, the logic behind B_{AOD} calculation has been validated in section 4.4.4. Suggesting, that with the known limitations, this was the best possible way for interpolating AOD with DEM. Now considering the height as a filter, AOD at 1300 m height in the grid was then extracted and considered as B_{AOD} (Figs. S2 and S3). Statistical cleaning, as mentioned above (section 4.4.1), was applied to the data set to avoid biases due to cloud cover or any other contaminations.

4.4.3. The Kathmandu Valley AOD ($KVal_{AOD}$)

Kathmandu city extends approximately between 1300 masl and 1400 masl in altitude, represented by the black dotted lines and red solid lines in the left and right panels of Fig. 3, respectively. Hence, to determine changes in pollution levels in the valley, it was necessary to subtract the background pollution. $KVal_{AOD}$ (representative of valley layer pollution levels) was derived after subtracting 'B_{AOD}' from 'K_{AOD}', as defined in Eqn (1).

4.4.4. Estimating low lying plain contribution to the background

In section 4.4.2 we hypothesized that the AOD at 1300 m elevation in the present context of mountainous regions might be advected from lowland AOD and be contributing as background. However, the percentage of lowland AOD contributed as background has yet to be quantified. Hence, we estimated the contribution of lowland AOD at 1300 m height and above, with respect to the total column, on a seasonal basis. Two methods were employed: (1) AOD at different heights were derived by integrating the CALIPSO aerosol extinction profiles and their contribution from 1300 m height and above to the total column, estimated on a seasonal basis; (2) AOD at different heights near Kathmandu (but excluding the points within Kathmandu) were derived and their seasonal contribution from 1300 m height with respect to the total column were estimated. Based on the seasonal contributions derived from the above methods, B_{AOD} was calculated from lowland AOD and compared with B_{AOD} defined in section 4.4.2.

4.4.4.1. Quantification of background contributions using CALIPSO extinction profiles. The pollution accumulated in the low lying plains, south of Kathmandu are a mixture of pollutants due to the sources located within the IGP region along with that transported from elsewhere (Fig. S5). The back trajectory analysis over IGP region (85.04°E longitude, 26.02°N latitude, 50 masl) arriving at 1200 m agl (above ground level) for winter (December 2013), summer (April 2013) and monsoon (July 2013) seasons have been shown in Fig. S5. This analysis indicates the different source regions of pollutants arriving over the IGP region. Therefore, any pollution transported to Kathmandu through the low lying plain regions in the South would definitely bring in the mixture of pollutants and dust from different sources in the region. In order to verify the same, synoptic wind patterns during selective months in the winter (December 2013), pre-monsoon (April 2013) and monsoon (July 2013) season over the South Asian region were plotted using ERA-interim reanalysis datasets at 850 hPa (Fig. S6). However, the reanalysis plots were not able to convey the exact information due to presence of high elevation places like Tibetan plateau, situated North of Kathmandu. Hence, we also performed another back trajectory analysis for the Kathmandu valley (85.31°E, 27.7°N; 100 m AGL) (Fig. S7) that depicted transport of air masses through western and southern regions. On majority of times, air masses arriving at Kathmandu were from the low lying plain regions, over which the subsequent analysis has been performed. Similar features of transported air masses from the southern and western directions were also observed in previous studies performed over the valley (Mahata et al., 2018; Putero et al., 2015). Therefore, we considered that, above 1300 m, aerosols are well mixed and advected toward the mountain region, so acting as background pollution. Hence, CALIPSO aerosol extinction coefficient profiles over a larger area in the IGP region (between latitude 25° and 27° and longitude 81–89°; green grid in Fig. 2) were used for the period 2006–2014. Seasonally, averaged aerosol extinction profiles were derived using all available profiles from the surface to 6 km height (Fig. 4). Column-integrated aerosol extinction profiles for the total column and for 1300 m and above

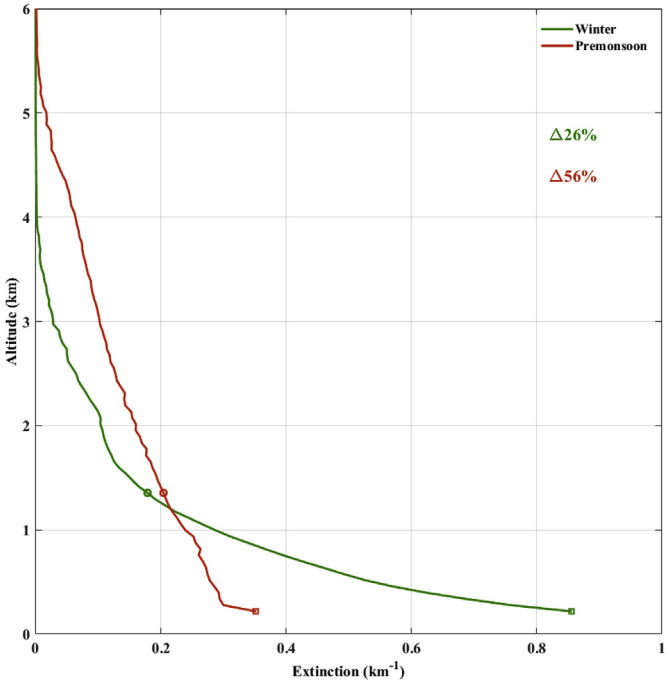

Fig. 4. Seasonal mean CALIPSO aerosol extinction profiles. ('□' symbols indicate integrated extinction of total column whereas 'o' symbols indicate integrated extinction at 1300 m height and above). Δ, percentage contribution of background to 1300 m and above in comparison to the total column for each season.

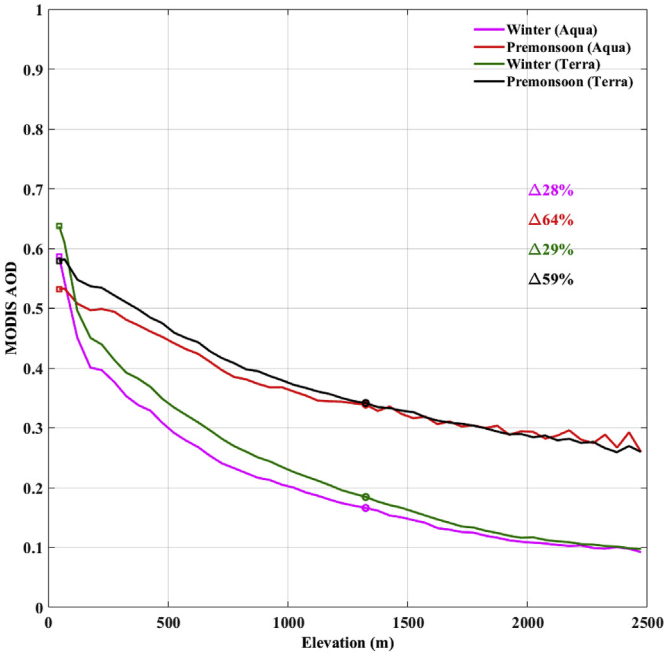

Fig. 5. Seasonal variation in MODIS Aqua and Terra AOD based on elevation. ('□' symbols indicate AOD low-elevation regions; 'o' symbols indicate AOD in elevated regions). 'Δ' represents percentage contribution of background to elevated region in each season.

were then derived. In this case the percentage of column integrated extinction fraction from 1300 m and above compared with the total column extinction fraction (from surface to top) will act as background integrated extinction for mountain regions at 1300 m and above (Kathmandu in the present case). Results indicated ~30% and 60% contributions from lowland AOD as background during the winter and pre-monsoon seasons, respectively. This percentage change is represented by a delta (Δ) in Fig. 4.

4.4.4.2. Quantifying background from AOD at different elevations. If the hypothesis in 4.3.4.1 is valid, then AOD values observed at different elevations in the nearby regions of Kathmandu will follow similar fraction contributions considering AOD in elevated region (terminology used for AOD at 1300 m height) and AOD in low-elevation region (terminology used for AOD at ~50 m height). In order to determine the fraction contribution of elevated region AOD in comparison to AOD at surface, we used AOD at different elevations in the 2° × 2° grid (latitude 26°–28° N and longitude 84°–86° E) surrounding Kathmandu, but excluding the points within Kathmandu during the study period (2000–2015). Seasonal average AOD profiles were derived based on their elevations. Considering mean AOD in low-elevation region, the seasonal contribution from elevated region AOD were determined for both Aqua and Terra (Fig. 5). Results from this analysis also indicated ~30% and 60% contribution of low-elevation region AOD at elevated region in winter and pre-monsoon seasons, respectively. A higher contribution of background during the pre-monsoon season might result from intense solar radiation affecting the surface, which creates deep convection and results in the lifting of surface aerosols to higher elevations/transport of dust. Such phenomena have also been observed at the high-altitude locations of Nainital (central Himalayan region) and Darjeeling (lower eastern Himalaya) in India (Chatterjee et al., 2012; Kumar et al., 2018).

4.4.4.3. Estimating background AOD (B_{AOD}) from fraction contribution of lowland AOD. In the above subsections (4.4.4.1 and 4.4.4.2) it was observed that ~30% and 60% of lowland AOD can be considered as background pollution at altitudes of 1300 m and above in winter and pre-monsoon seasons respectively. The hypothesis that a certain amount of pollution from low laying plains penetrate into Kathmandu as background might thus be valid. Based on the percentage contribution of lowland AOD at 1300 m and above, B_{AOD} was calculated as in Eqns (2) and (3) on a monthly basis:

$$\textit{Summer Background AOD at } 1300\ m = \textit{Summer lowland AOD} \times 60\% \quad (2)$$

$$\textit{Winter Background AOD at } 1300\ m = \textit{Winter lowland AOD} \times 30\% \quad (3)$$

If the B_{AOD} derived from lowland AOD using Eqns (2) and (3) is similar to the B_{AOD} derived near Kathmandu at 1300 m elevation, this would justify our assumption of background calculation made in section 4.4.2, as well as validate our assumption of lowland AOD as a source of background. We therefore, compared the B_{AOD} derived from lowland AOD with B_{AOD} retrieved at 1300 m height near Kathmandu (section 4.4.2). A scatter plot between two variables indicates the existence of certain relation between them. A narrower scatter indicates, stronger correlation between the variables being studied. While, a broader scatter indicates some levels of uncertainty based on the correlation coefficient. In the present case a moderate correlation between B_{AOD} derived by both means (with a slope near to 1; Fig. 6) justify our calculations of B_{AOD}. However, a larger scatter indicates the presence of uncertainties in the comparison. Seasonally averaged CALIPSO profiles for 9 years (2006–2014) were used to understand the column-integrated aerosol extinction in the low laying plains. The fractional contribution from above 1300 m to total extinction was considered from the mean profiles to interpolate the B_{AOD} derived from the lowland AOD. We used constant fractions of 30% and 60% during the winter and summer seasons respectively to quantify the B_{AOD} from lowland AOD. However, these constant fractions, are based on climatological mean profiles rather than daily profiles. The reason being CALIPSO cannot provide daily vertical aerosol extinction profiles and has limited spatial and temporal retrievals over the selected region. Since we took climatological mean data, some level of uncertainties

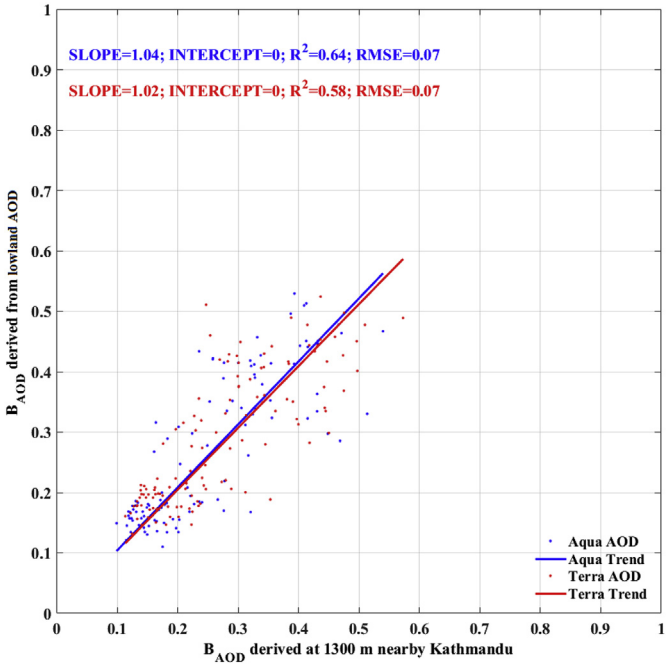

Fig. 6. Comparison of background aerosol optical depth (B_{AOD}) from lowland AOD and B_{AOD} from near Kathmandu at 1300 m elevation.

were expected in the inability to capture the day to day variability in vertical aerosol distribution. This will also lead to uncertainties in quantifying the B_{AOD} from CALIPSO data on a day to day basis. Apart from that the 3 km AOD data product used for estimating B_{AOD} also has certain amount of uncertainty due to grid elevations. Hence, due to the uncertainties in the aerosol extinction profiles from CALIPSO and grid AOD retrievals, the data points have a large scatter but they are well aligned on the slope (closer to 1 with a moderate correlation), indicating that the logic for calculating B_{AOD} was valid.

5. Results and discussion

5.1. K_{AOD} trend

Fig. 7 represents the time series of monthly and annual AOD derived from MODIS Aqua (a) and Terra (b). Throughout the study, only AOD data from winter (November, December, January and February) and summer (March, April, May and June) months were considered for analysis. Data points during the monsoon period (July, August, September and October) were extremely scarce and influenced by increased cloud. Using these values for the analysis could have introduced undesired biases, and so we did not use monsoon data in this study. AOD derived from MODIS onboard Terra and Aqua during 2000–2015 and 2003–2015, respectively, suggested an increase of approximately 35% over Kathmandu. The annual percentage increase in MODIS AOD during the study period from both Terra and Aqua data was ~6–7% per year. The significance of the annual trend in K_{AOD} was determined by undertaking a Kendall's tau-b (τ_b) correlation between years and annual AOD values. A strong, positive and statistically significant correlation was observed between annual AOD and years ($\tau_b = 0.78$, $p = 0.0001$ for AQUA and $\tau_b = 0.88$, $p = 0.0000$ for TERRA). These increasing trends in AOD could be linked to the rapid increase in population, vehicles and energy demands, as discussed in section 1. To further compare the change in AOD between the initial and final year of observation, frequency distribution curves for AOD from Aqua and Terra between 2003 and 2015, and between 2001 and 2015, respectively, are shown in Fig. 8. The peak values of the initial and final years in the AOD distribution curve point toward a shift from ~0.2 to ~0.4 in both cases. This shift is an indicator of deterioration in local columnar aerosol loading between the initial and final years of this study (1.5 decades). The observed increasing trend in AOD can be attributed to two major components: the changes in background pollution levels and the Kathmandu Valley levels. This makes the determination of B_{AOD} an important issue.

5.2. $KVal_{AOD}$ trend

To quantify the growth in pollution in the valley layer only, we have to subtract B_{AOD} as discussed in section 4.4.2 from the K_{AOD} as discussed in section 4.4.1 in order to derive the $KVal_{AOD}$. The increasing trend in $KVal_{AOD}$, with monthly and annual data points, is shown in Fig. 9. Annual mean $KVal_{AOD}$ during 2001 and 2003 for Terra and Aqua was 0.104 and 0.126, respectively; while that for the year 2015 for Terra and Aqua was 0.177 and 0.188, respectively. These figures indicate the rise in pollutant levels in the city over a period of 1.5 decades. Trend analysis of $KVal_{AOD}$ (Fig. 9) during the study period suggests an increase of approximately 50–60%. Kendall's tau-b (τ_b) correlation test indicated a strong, positive and statistically significant correlation between the annual average $KVal_{AOD}$ and years ($\tau_b = 0.62$, $p = 0.003$ for AQUA and $\tau_b = 0.64$, $p = 0.001$ for TERRA).

5.3. Estimating the contribution of background pollution at the Kathmandu Valley layer

Understanding the valley layer pollution exposure is vital because of its influence on the 1,309,000 people living there (Web Reference 1). In the previous sections 4.4.1–5.1 we discussed columnar pollution issues, which present a completely different scenario to that of valley layer pollution (within 1300–1400 m). The $KVal_{AOD}$ discussed in the previous section 5.2 is representative of the pollution in the valley, except for the additional contribution from background pollution at this layer, which was subtracted earlier (as discussed in section 5.2). Hence, it is important to quantify the additional contribution from background in the Kathmandu Valley only. To quantify the additional contribution, we employed three approaches: (1) derive the contribution of background pollution at the Kathmandu Valley layer using CALIPSO extinction profiles; (2) use in-situ PM observation data from Kathmandu city and a background location (Dhulikhel); and (3) model simulations to estimate an 'on and off' Kathmandu emission scenario.

5.3.1. Background contribution at the Kathmandu Valley layer using CALIPSO profiles

We used CALIPSO extinction profiles to quantify the contribution of background pollution at the Kathmandu Valley layer. Using seasonal CALIPSO profiles, we calculated the integrated aerosol extinction fraction between 1300 m and 1400 m elevation and derived it's percent contribution to the total lowland column (Fig. 3; right panel). The background contribution at the valley layer was denoted by $BVal_{AOD}$. It was observed that ~5% of pollutants (4.84% in winter and 5.41% in summer) of the total lowland column was translated into the Kathmandu Valley layer. Hence, assuming that ~5% of lowland AOD is mixed with emissions of the Kathmandu Valley, $BVal_{AOD}$ is calculated as in Eqn (4):

$$BVal_{AOD} at\ 1300\ m\ to\ 1400\ m\ layer = 5\% \times lowland\ AOD \quad (4)$$

Using the above mentioned equation (Eqn (4)), the contribution of $BVal_{AOD}$ to the Kathmandu Valley pollution levels was determined for the initial and final years of the study from Aqua and Terra between 2003 and 2015, and between 2001 and 2015 respectively. Mean AOD during 2015 for Terra at the low elevation region (50 m height; representing lowland AOD) was ~0.61 and ~0.74 in summer and winter, respectively. Hence, 5.41% in summer and 4.84% in winter of this mean AOD would represent the background pollution (that advects from the low laying plain region), which additionally combines with

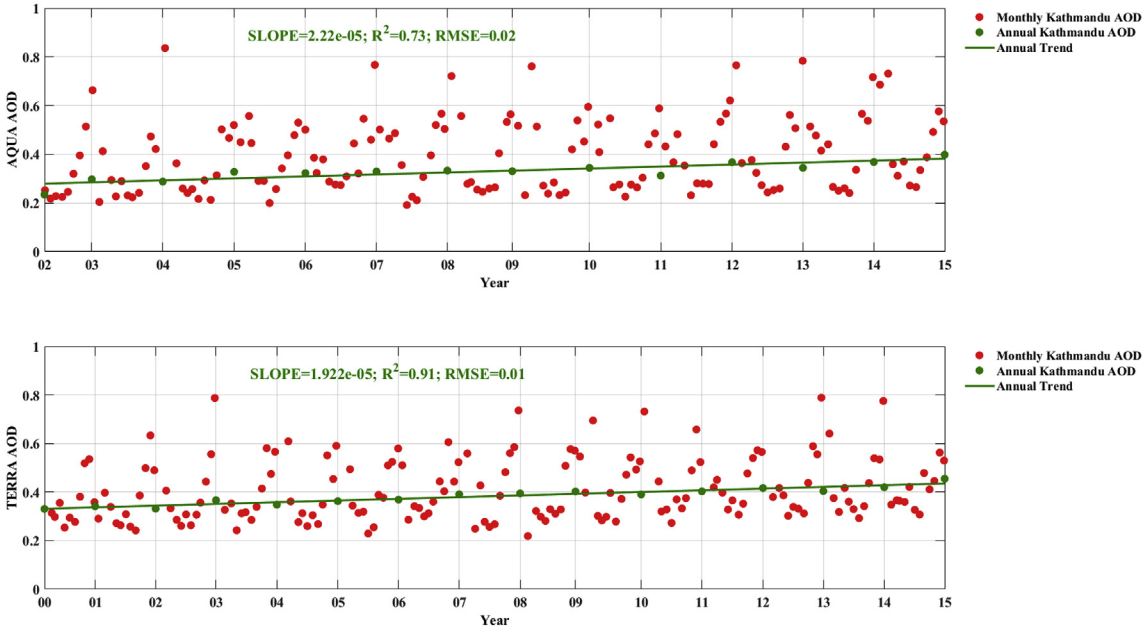

Fig. 7. Annual trend of Kathmandu aerosol optical depth (K_{AOD}) indicating ~35% increase between the initial and final years of the study. Top panel: trend for Aqua AOD from 2002 to 2015; bottom panel: trend for Terra AOD from 2000 to 2015.

emissions from within the valley. The $BVal_{AOD}$ was estimated to be ~0.033 in summer and ~0.036 in winter. Mean $KVal_{AOD}$ determined in the previous section 5.2 was ~0.185 in summer and ~0.191 in winter for 2015. The percentage contribution of $BVal_{AOD}$ to $KVal_{AOD}$ was found to be ~18% (mean summer and winter). This indicates that 18% of pollutants from the low laying plain region was advected to Kathmandu as background pollution during 2015. These results were closer match with few observations made previously at different locations in the valley (section 3). A decrease in air pollution levels by ~60–70% was observed between the valley center/urban sites and periphery/background sites, indicating high pollution sources in the valley and a lesser contribution from the background (Aryal et al., 2009, 2008; Stone et al., 2010). The background contribution at the valley layer was calculated for the years 2001 and 2015, and for 2003 and 2015, using data from Terra and Aqua, respectively (Table 2). The results indicate that between the 2001 and 2003 base years taken for Aqua and Terra and 2015 (the final year of study) there was a decline in contributions from background pollution to Kathmandu Valley pollution levels. This contribution was in the range of ~25–29% in the initial years to ~18% in the final years, which is also consistent with the rise in the Kathmandu Valley pollution levels (Fig. 9).

5.3.2. Background contribution to the Kathmandu Valley from in-situ observations

Our second approach to estimating the contribution of background pollution was by using in-situ observations of PM: to compare Kathmandu Valley pollution levels with those of a background location. Ratnapark was chosen as the in-valley location, while Dhulikhel was chosen as a background location with respect to Kathmandu (particularly when the winds are not westerly, i.e. when Dhulikhel was not downwind of Kathmandu) Fig. 2. The Department of Environment (DoEnv), Ministry of Population and Environment, Nepal, in partnership with the International Center for Integrated Mountain Development (ICIMOD), set up an advanced air quality monitoring station at both locations. PM at both locations was measured using environmental dust monitors (GRIMM-EDM-180D, Grimm Aerosol Technik GmbH & Co. Kg, Dorfstrasse-9, Germany). These instruments were brand new and factory calibrated at the time of deployment. Comparison of PM_{10} concentration from Dhulikhel (when the winds are not westerly, i.e. when Dhulikhel was not downwind of Kathmandu) and Ratnapark were made for two representative months (April for summer and November for winter). As Dhulikhel is situated east of Kathmandu Valley, the PM_{10} values for winds from a westerly direction (270–315°) were removed from further analysis to avoid any biases. The difference between the

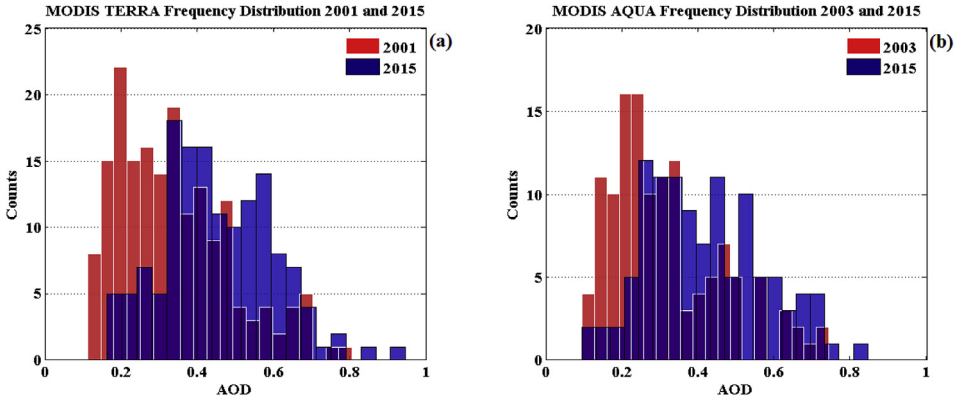

Fig. 8. Frequency distribution for (a) MODIS Terra in 2001 and 2015; (b) MODIS Aqua in 2003–2015. The comparison did not take into account the starting year of Terra (2000) and Aqua (2002) as there was some data loss.

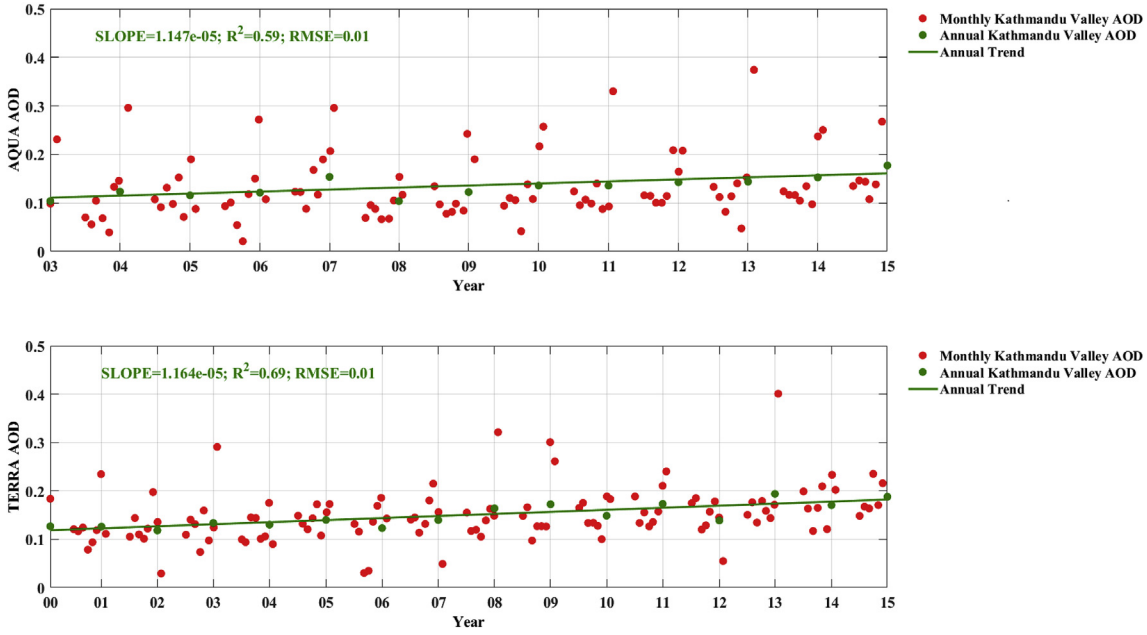

Fig. 9. Annual trend of Kathmandu Valley aerosol optical depth ($KVal_{AOD}$) between the initial and final years of the study. Top panel: scatter plot of Aqua AOD from 2003 to 2015; bottom panel: scatter plot of Terra AOD from 2000 to 2015.

Table 2
Background contribution to Kathmandu Valley aerosol optical depth ($KVal_{AOD}$).

MODIS Terra AOD analysis				
2015				Mean
Summer lowland AOD	0.61	Winter lowland AOD	0.74	
Summer $BVal_{AOD}$	0.033	Winter $BVal_{AOD}$	0.036	
Summer $KVal_{AOD}$	0.185	Winter $KVal_{AOD}$	0.191	
% Bkg cont. summer	17.83	% Bkg cont. winter	18.77	18.30
2001				**Mean**
Summer lowland AOD	0.64	Winter lowland AOD	0.61	
Summer $BVal_{AOD}$	0.035	Winter $BVal_{AOD}$	0.030	
Summer $KVal_{AOD}$	0.14	Winter $KVal_{AOD}$	0.113	
% Bkg cont. summer	24.86	% Bkg cont. winter	26.14	25.50
MODIS Aqua AOD analysis				
2015				**Mean**
Summer lowland AOD	0.57	Winter lowland AOD	0.67	
Summer $BVal_{AOD}$	0.031	Winter $BVal_{AOD}$	0.032	
Summer $KVal_{AOD}$	0.216	Winter $KVal_{AOD}$	0.138	
% Bkg cont. summer	14.20	% Bkg cont. winter	23.29	18.75
2003				**Mean**
Summer lowland AOD	0.56	Winter lowland AOD	0.54	
Summer $BVal_{AOD}$	0.030	Winter $BVal_{AOD}$	0.026	
Summer $KVal_{AOD}$	0.136	Winter $KVal_{AOD}$	0.071	
% Bkg cont. summer	22.37	% Bkg cont. winter	36.48	29.42

Note: % Bkg cont: is the percentage contribution of $BVal_{AOD}$ to the $KVal_{AOD}$.

PM concentrations of these two locations provided a vivid picture of the background contribution to the Kathmandu Valley (Fig. 10). Analysis of daily average data points indicated approximately 30% contribution from the background during both summer and winter seasons (Fig. 10). Results from these observations were also similar to our results of background contribution of ~20–25% derived from AOD values, confirming our results from satellite-derived AOD analysis.

5.3.3. Determination of background contribution using chemical transport models

The third approach was to compare background contributions to valley aerosol load using results obtained from two chemical transport models. Our approach was to zero out emission in the Kathmandu Valley and derive the residual pollution levels, which would represent the background contribution to surface pollution. In the present study both models were simulated for the Kathmandu 'on' and 'off' scenarios for $PM_{2.5}$. WRF-CHEM was also simulated for AOD and WRF-STEM with region tagged CO tracer was used for estimating anthropogenic CO contributions of the different region to the Kathmandu Valley. We would like to highlight here that detailing the model results was not a primary objective of this paper; we only wished to observe how well the models worked in the Kathmandu Valley so that future studies could be enhanced.

Results obtained from both model runs are shown in Fig. 11 (top and middle panel for WRF-CHEM and bottom panel for WRF-STEM). WRF-CHEM and WRF-STEM runs for $PM_{2.5}$ indicated ~73–85% of the pollution coming from the background in summer and ~46–75% in winter, respectively. When taking AOD into account, ~90% was estimated to come from the background during the summer, while that for the winters was ~75% from the WRF-Chem runs. Overall, these figures indicate that ~50–85% of $PM_{2.5}$ came from the background. While 75–90% of AOD was due to the background. These results showed a relatively high level of pollution coming from background, which was close neither to the in-situ observations nor to the AOD analysis-based results. When compared with earlier studies undertaken within the valley and valley background sites over a short period of time (Aryal et al., 2009; Stone et al., 2010), the model-derived results underestimated the contribution of the Kathmandu Valley pollution. The primary reasons for such an underestimation lies with the use of older emission inventories and complex topography of the region. The emission inventories used for the model were constructed way back in 2010 and have not been updated till date. However, a rapid growth in the population and energy demands within the valley must have significantly increased the concentration of pollutants in the present times but has not been represented properly in the emission inventories. Hence, the models highly underestimate the valley pollution levels. A recent study evaluating modeled BC concentrations with measurements

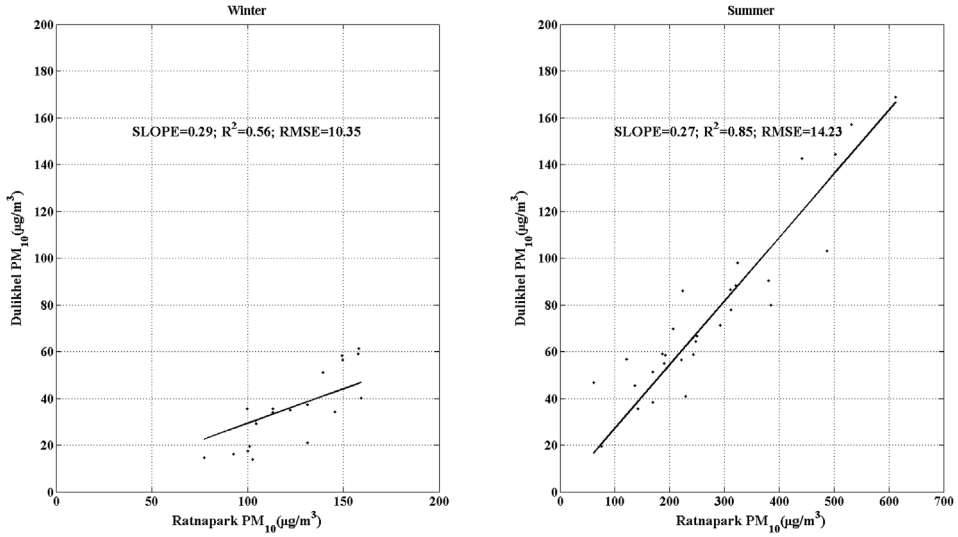

Fig. 10. Seasonal scatterplot for Dhulikhel and Ratnapark for determining background contribution to the Kathmandu Valley pollution.

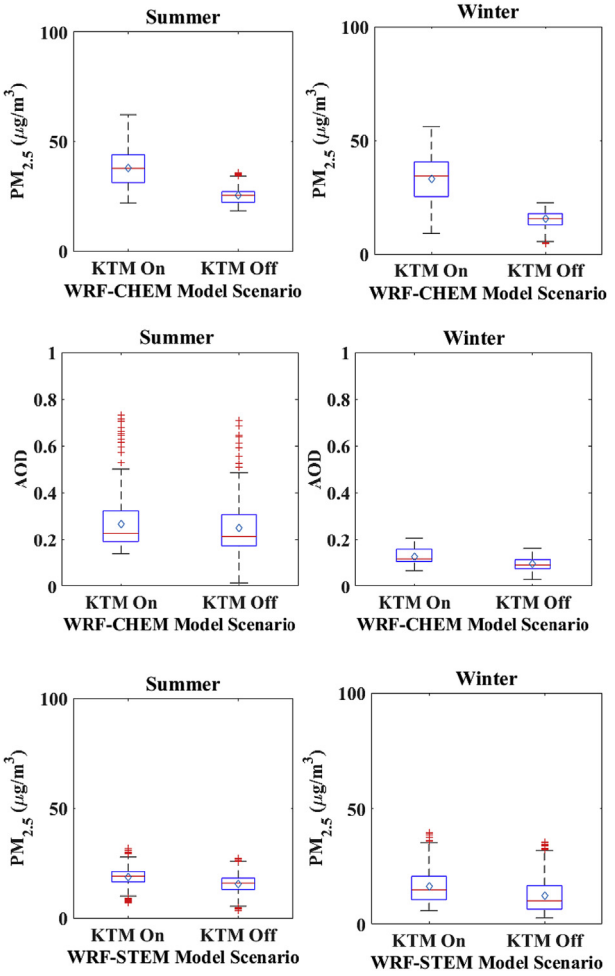

Fig. 11. Graphs showing contribution of background pollution to Kathmandu Valley pollution using WRF-CHEM and WRF-STEM simulations. Simulations were conducted for two scenarios: Kathmandu Valley emissions on, and off. It was assumed that, when the Kathmandu Valley emissions were off, whatever remained was from background pollution.

within the Kathmandu Valley also suggested an underestimation of BC by 89 and 82% respectively in February and May (Mues et al., 2018). Another study performed by Zhong et al. (2018) indicated a strong underestimation of PM emission from the road and transport sector in the HTAP_v2.2 emission inventory. They used a recent international Vehicle Emission (IVE) model to update emissions from vehicles and observed IVE estimated emissions to be 375 times higher for EC in comparison to that of HTAP. After making modifications to the existing inventories, the total emission from all sectors in the study compared with that of HTAP in 2010 (ton month^{-1}) showed a significant increase in CO, EC and $PM_{2.5}$ by ~50, 550 and 240%. Hence, large underestimation in the pollutant concentrations within the valley is expected by the use of an older emission inventory. Also a complex terrain would create enough biases within the model rendering it incapable of capturing mountain meteorology and thus creating errors in estimation of different pollutants. Study by Mues et al. (2018) also indicated difficulties in estimating different meteorological parameters within the Kathmandu Valley. They observed 10% overestimation in planetary boundary layer. Hence, the findings from the present study and discussions with other studies indicate the requirement of fine resolution emission inventories along with stronger modeling initiatives that can take into account the complex topography and meteorology of the Himalayan region. Incorporation of local emission estimates from under represented sources like diesel pumps ('terai' region), charcoal production (community forest regions), garbage burning (rural-urban location) etc. would definitely add on for better modeling outputs over the Kathmandu Valley and the Himalayan region in general.

5.3.4. *Identifying source contribution*

The WRF-STEM model with region tagged CO-Tracer was used to simulate the anthropogenic CO concentration of Kathmandu valley from different source regions. Few studies in the recent past have also used this approach for quantifying the contribution of different source regions over Lumbini (Rupakheti et al., 2017) and Central Asia (Kulkarni et al., 2015). The pie chart (Fig. 12) indicates that only 19% and 45% contribution was from within the valley (KTM_CO) in the pre-monsoon and winter season respectively while that from background was 81–55%. The quantitative findings for anthropogenic CO emissions from the model output suggest 225.7 ppbv and 138.7 ppbv during pre-monsoon and winter respectively for the Kathmandu Valley. While that of observation undertaken during the same period at Bode (in Kathmandu Valley), indicates 770 ppbv and 819.7 ppbv of CO during the pre-monsoon and winter season respectively (Mahata et al., 2018). This indicated that the model underestimated the CO concentration by ~4 times. The model estimated Kathmandu valley CO concentration (excluding background) was 43.7 ppbv and 62.7 ppbv respectively for pre-monsoon and winter. These result indicate that the model is not being

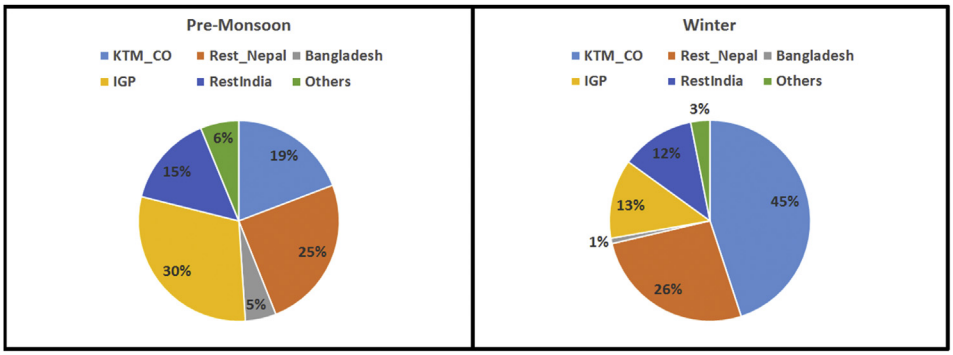

Fig. 12. Various source region contributions to the average CO concentration in the Kathmandu Valley using WRF-STEM model (left panel) summer season (right panel) winter season.

able to capture the Kathmandu valley emissions appropriately. Similar results of high underestimation of BC and EC within the valley was observed by Mues et al. (2018); Zhong et al. (2018). Hence, indicating towards a strong requirement to update the existing emission inventories by incorporating local estimates and at a finer resolution and simultaneously enhance the model capacities for fine scale modeling".

5.4. Influence of background air pollution on visibility in particular months

Visibility is an urban air quality issue that impacts the daily lives of the people in the valley. Within the troposphere, visibility is primarily limited by scattering of solar radiation in the presence of aerosols (Seinfeld and Pandis, 2006). On some days there are drastic changes in long-distance visibility in Kathmandu. Fig. 13 shows photographs taken on two days at the end of February and beginning of March. One illustrates a clear view of the Himalayan ranges (Fig. 13(a)), but there is no clear view in the other (Fig. 13(b)). To understand the role on visibility of background and Kathmandu Valley pollution levels, we verified the AOD values for those two particular days. On the clear day (28 February 2013) the $KVal_{AOD}$ was 0.06 from Aqua (Terra data were unavailable that day) and was similar to the B_{AOD} (0.07). On the hazy day (2 March 2013) the $KVal_{AOD}$ was ~0.08 and 0.03 from Aqua and Terra, respectively, but B_{AOD} was ~0.29 and 0.33, respectively. This indicates that, in Kathmandu, long-distance visibility in certain months may be affected by the background pollution levels.

To study the role of pollutants and their relationship to visibility it is essential to have a clear understanding of local and regional pollution, and the influence of meteorology. Our previous analysis indicates that the contribution of background pollution is higher in summer months (section 4.4.4.1 and 4.4.4.2). In winter, strong inversion conditions makes visibility conditions poor in the valley. Hence, to study the impacts of visibility and relate it to valley/background pollution levels, we chose the month of February when winter is almost over and summer has yet to begin. A study was undertaken to correlate K_{AOD} and $KVal_{AOD}$ with visibility for all days in February during 2010–2014 (Fig. 14). Visibility data for Tribhuvan International Airport, in the center of the Kathmandu Valley, were acquired from the Global Surface Hourly database of the National Climatic Data Center (NCDC) (https://www7.ncdc.noaa.gov/CDO/cdo). These data sets have been widely used to estimate the impacts of visibility change in a South Asian context (Lee et al., 2016), providing a strong basis for using this specific data set. Visibility showed a negative trend with K_{AOD} but no particular trend with $KVal_{AOD}$. This suggests the dominant role of background pollution in influencing visibility in certain months.

6. Conclusions

1. K_{AOD} suggests an increase in pollution load by ~35% during the 1.5 decades of the present study.
2. The study suggests that ~30% and 60% of the lowland AOD column was contributed as background to the Kathmandu column during winter and pore-monsoon season respectively.
3. The $KVal_{AOD}$ derived after subtracting B_{AOD} from K_{AOD} suggests an increasing trend of ~50–60% during the study period.
4. Using vertical aerosol extinction profiles, the contribution of surface/lowland AOD at the Kathmandu Valley layer (1300 m - 1400 m) was observed to be ~5%.
5. Considering ~5% of lowland AOD being translated at the Kathmandu Valley layer, B_{AOD} was found to add a pollutant load of approximately 20–25% to the $KVal_{AOD}$. Observation based results were a closer match to satellite derived percentage contribution for background. While model based results highly underestimated the local Kathmandu Valley contribution.
6. Absence of fine resolution and updated emission inventories result in underestimation of pollution load within the Kathmandu Valley. Apart from this there is also a strong need for developing model capacities to capture topography at a finer resolution.
7. The decline in visibility in certain months was observed to be

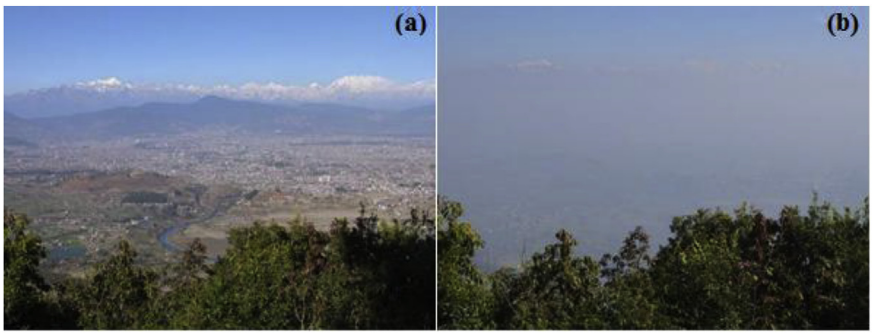

Fig. 13. View of Himalayan ranges from Hattiban Resort, Nepal, on (a) 28 February 2013 (a clear day when the Himalayan ranges could be seen); and (b) 2 March 2013 (a hazy day when the Himalayan ranges could not be seen).

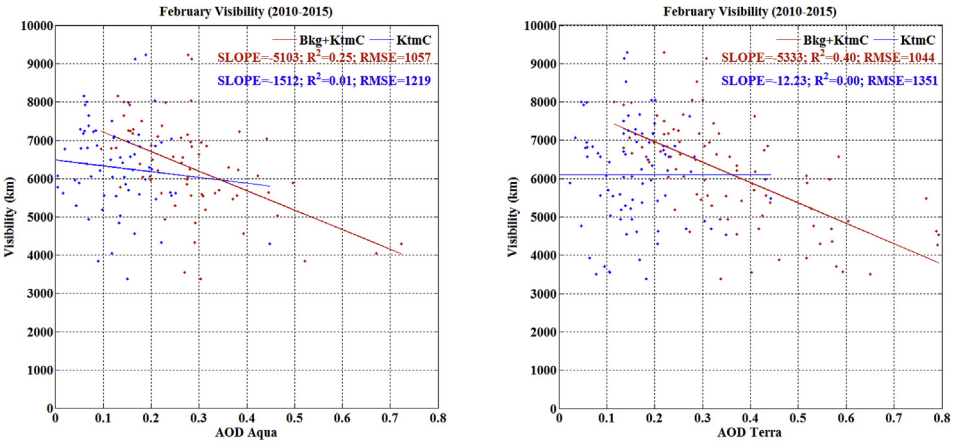

Fig. 14. Correlation of visibility with $KVal_{AOD}$ (blue coloured lines) and correlation of visibility with K_{AOD} and background AOD integrated together (red coloured lines) for the months of February between 2010 and 2015. Left panel: correlation of AOD from MODIS Aqua; right panel correlation of AOD from MODIS Terra. (For interpretation of the references to colour in this figure legend, the reader is referred to the Web version of this article.)

affected by changes in background pollution levels.

Competing financial interests

The authors declare that they have no actual or potential competing financial interests.

Acknowledgements

This study was partially supported by the core funds of ICIMOD contributed by the governments of Afghanistan, Australia, Austria, Bangladesh, Bhutan, China, India, Myanmar, Nepal, Norway, Pakistan, Sweden and Switzerland. The views and interpretations in this publication are those of the authors and are not necessarily attributable to their organizations. Acknowledgements are also due to Elaine Monaghan for English editing of the manuscript. The Aqua and Terra MODIS AOD product was acquired from the Level-1 and Atmosphere Archive & Distribution System (LAADS) Distributed Active Archive Center (DAAC), located in the Goddard Space Flight Center in Greenbelt, Maryland, USA (https://ladsweb.nascom.nasa.gov/). We acknowledge the ECCAD team for the archiving and distribution of the emission inventory datasets. The GIOVANNI online platform and NASA are acknowledged for making available earth science related data sets. NOAA's NCDC is acknowledged for maintaining the site and making the data freely available. We acknowledge use of the WRF-Chem preprocessor tools (mozbc, fire_emiss, bio_emiss, and anthro_emiss) provided by the Atmospheric Chemistry Observations and Modeling Lab (ACOM) of NCAR at https://www2.acom.ucar.edu/wrf-chem/wrf-chem-tools-community. We also acknowledge use of NCAR/ACOM MOZART-4 global model output available at http://www.acom.ucar.edu/wrf-chem/mozart.shtml. The authors would like to thank both the anonymous reviewers, whose reviews were extremely helpful in enhancing the quality of the manuscript. We would also like to convey our gratitude to the editor for smooth handling of the manuscript.

Appendix A. Supplementary data

Supplementary data to this article can be found online at https://doi.org/10.1016/j.atmosenv.2018.12.043.

References

Adhikary, B., Carmichael, G.R., Tang, Y., Leung, L.R., Qian, Y., Schauer, J.J., Stone, E.A., Ramanathan, V., Ramana, M.V., 2007. Characterization of the seasonal cycle of south Asian aerosols: a regional-scale modeling analysis. J. Geophys. Res. 112, D22S22. https://doi.org/10.1029/2006JD008143.

Adhikary, B., Carmichael, G.R., Kulkarni, S., Wei, C., Tang, Y., D'Allura, a., Mena-Carrasco, M., Streets, D.G., Zhang, Q., Pierce, R.B., Al-Saadi, J. a., Emmons, L.K., Pfister, G.G., Avery, M. a., Barrick, J.D., Blake, D.R., Brune, W.H., Cohen, R.C., Dibb, J.E., Fried, a., Heikes, B.G., Huey, L.G., O'Sullivan, D.W., Sachse, G.W., Shetter, R.E., Singh, H.B., Campos, T.L., Cantrell, C. a., Flocke, F.M., Dunlea, E.J., Jimenez, J.L., Weinheimer, a. J., Crounse, J.D., Wennberg, P.O., Schauer, J.J., Stone, E. a., Jaffe, D. a., Reidmiller, D.R., 2010. A regional scale modeling analysis of aerosol and trace gas distributions over the eastern Pacific during the INTEX-B field campaign. Atmos. Chem. Phys. 10, 2091–2115. https://doi.org/10.5194/acp-10-2091-2010.

Aryal, R.K., Lee, B.-K., Karki, R., Gurung, A., Kandasamy, J., Pathak, B.K., Sharma, S., Giri, N., 2008. Seasonal PM10 dynamics in Kathmandu Valley. Atmos. Environ. 42, 8623–8633. https://doi.org/10.1016/j.atmosenv.2008.08.016.

Aryal, R.K., Lee, B.K., Karki, R., Gurung, A., Baral, B., Byeon, S.H., 2009. Dynamics of PM2.5 concentrations in Kathmandu Valley, Nepal. J. Hazard Mater. 168, 732–738. https://doi.org/10.1016/j.jhazmat.2009.02.086.

Bhardwaj, P., Naja, M., Rupakheti, M., Panday, A.K., Kumar, R., Mahata, K., Lal, S., Chandola, H.C., Lawrence, M.G., 2017. Variations in surface ozone and carbon monoxide in the Kathmandu Valley and surrounding broader regions during SusKat-ABC field campaign: Role of local and regional sources. Atmos. Chem. Phys. Discuss. 1–49. https://doi.org/10.5194/acp-2017-306.

Cakmak, S., Dales, R.E., Vidal, C.B., 2007. Air pollution and mortality in Chile: Susceptibility among the elderly. Environ. Health Perspect. 115, 524–527. https://doi.org/10.1289/ehp.9567.

Central Bureau of Statistics Nepal, 2012. National Population and Housing Census 2011. National Report. Government of Nepal.

Central Bureau of Statistics of Nepal- economic demography, 2014. Population Monograph.

Chatterjee, A., Ghosh, S.K., Adak, A., Singh, A.K., Devara, P.C.S., Raha, S., 2012. Effect of Dust and Anthropogenic Aerosols on Columnar Aerosol Optical Properties over Darjeeling (2200 m asl), Eastern Himalayas, India. PLoS One 7, e40286. https://doi.org/10.1371/journal.pone.0040286.

Davidson, C.I., Lin, S.F., Osborn, J.F., Pandey, M.R., Rasmussen, R. a, Khalil, M. a, 1986. Indoor and outdoor air pollution in the Himalayas. Environ. Sci. Technol. 20, 561–567. https://doi.org/10.1021/es00148a003.

Emmons, L.K., Walters, S., Hess, P.G., Lamarque, J.F., Pfister, G.G., Fillmore, D., Granier, C., Guenther, A., Kinnison, D., Laepple, T., Orlando, J., Tie, X., Tyndall, G., Wiedinmyer, C., Baughcum, S.L., Kloster, S., 2010. Description and evaluation of the Model for Ozone and Related chemical Tracers, version 4 (MOZART-4). Geosci. Model Dev. (GMD) 3, 43–67. https://doi.org/10.5194/gmd-3-43-2010.

Giri, D., Murthy, V.,K., Adhikary, P.R., Khanal, S.N., 2006. Ambient air quality of Kathmandu valley as reflected by atmospheric particulate matter concentrations (PM 10). Int. J. Environ. Sci. Tech. 3, 403–410.

Gómez-Arroyo, S., Cortés-Eslava, J., Loza-Gómez, P., Arenas-Huertero, F., Grutter de la Mora, M., Morton Bermea, O., 2017. In situ biomonitoring of air quality in rural and urban environments of Mexico Valley through genotoxicity evaluated in wild plants. Atmos. Pollut. Res. https://doi.org/10.1016/j.apr.2017.06.009.

Guenther, A.B., Jiang, X., Heald, C.L., Sakulyanontvittaya, T., Duhl, T., Emmons, L.K., Wang, X., 2012. The Model of Emissions of Gases and Aerosols from Nature version 2.1 (MEGAN2.1): an extended and updated framework for modeling biogenic emissions. Geosci. Model Dev. (GMD) 5, 1471–1492. https://doi.org/10.5194/gmd-5-1471-2012.

Gul, C., Puppala, S.P., Kang, S., Adhikary, B., Zhang, Y., Ali, S., Li, Y., Li, X., 2018. Concentrations and source regions of light-absorbing particles in snow/ice in northern Pakistan and their impact on snow albedo. Atmos. Chem. Phys. 18, 4981–5000. https://doi.org/10.5194/acp-18-4981-2018.

Gupta, P., Remer, L.A., Levy, R.C., Mattoo, S., 2018. Validation of MODIS 3 km land aerosol optical depth from NASA's EOS Terra and Aqua missions. Atmos. Meas. Tech. 11, 3145–3159. https://doi.org/10.5194/amt-11-3145-2018.

Gurung, A., Bell, M.L., 2012. Exposure to airborne particulate matter in Kathmandu Valley, Nepal. J. Expo. Sci. Environ. Epidemiol. 22, 235–242. https://doi.org/10.1038/jes.2012.14.

Hastings, D.A., Dunbar, P.K., 1999. Global Land One-kilometer Base Elevation (GLOBE) Digital Elevation Model, Documentation, Volume 1.0. Key to Geophysical Records Documentation (KGRD), 34. 325 Broadway, Boulder, Colorado 80303, U.S.A.

He, Q., Zhang, M., Huang, B., Tong, X., 2017. MODIS 3 km and 10 km aerosol optical depth for China: Evaluation and comparison. Atmos. Environ. 153, 150–162. https://doi.org/10.1016/j.atmosenv.2017.01.023.

Janssens-Maenhout, G., Dentener, F., Aardenne, J. Van, Monni, S., Pagliari, V., Orlandini, L., Klimont, Z., Kurokawa, J., Akimoto, H., Ohara, T., Wankmüller, R., Battye, B., Grano, D., Zuber, A., Keating, T., 2012. EDGAR-HTAP: a harmonized gridded air pollution emission dataset based on national inventories. JRC Scientific and Technical Reportshttps://doi.org/10.2788/14102.

Jayarathne, T., Stockwell, C.E., Bhave, P.V., Praveen, P.S., Rathnayake, C.M., Islam, M.R., Panday, A.K., Adhikari, S., Maharjan, R., Goetz, J.D., DeCarlo, P.F., Saikawa, E., Yokelson, R.J., Stone, E.A., 2018. Nepal Ambient Monitoring and Source Testing Experiment (NAMaSTE): emissions of particulate matter from wood- and dung-fueled cooking fires, garbage and crop residue burning, brick kilns, and other sources. Atmos. Chem. Phys. 18, 2259–2286. https://doi.org/10.5194/acp-18-2259-2018.

Kim, B.M., Park, J.-S.S., Kim, S.-W.W., Kim, H., Jeon, H., Cho, C., Kim, J.-H.H., Hong, S., Rupakheti, M., Panday, A.K., Park, R.J., Hong, J., Yoon, S.-C.C., 2015. Source apportionment of PM10 mass and particulate carbon in the Kathmandu Valley, Nepal. Atmos. Environ. 123, 190–199. https://doi.org/10.1016/j.atmosenv.2015.10.082.

Kitada, T., Regmi, R.P., 2003. Dynamics of Air Pollution Transport in Late Wintertime over Kathmandu Valley, Nepal: As Revealed with Numerical Simulation. J. Appl. Meteorol. 42, 1770–1798. 10.1175/1520-0450(2003)042%3c1770:DOAPTI%3e2.0.CO;2.

Kulkarni, S., Sobhani, N., Miller-Schulze, J.P., Shafer, M.M., Schauer, J.J., Solomon, P.A., Saide, P.E., Spak, S.N., Cheng, Y.F., Denier van der Gon, H.A.C., Lu, Z., Streets, D.G., Janssens-Maenhout, G., Wiedinmyer, C., Lantz, J., Artamonova, M., Chen, B., Imashev, S., Sverdlik, L., Deminter, J.T., Adhikary, B., D'Allura, A., Wei, C., Carmichael, G.R., 2015. Source sector and region contributions to BC and $PM_{2.5}$ in Central Asia. Atmos. Chem. Phys. 15, 1683–1705. https://doi.org/10.5194/acp-15-1683-2015.

Kumar, A., Singh, N., Anshumali, Solanki, R., 2018. Evaluation and utilization of MODIS and CALIPSO aerosol retrievals over a complex terrain in Himalaya. Remote Sens. Environ. 206, 139–155. https://doi.org/10.1016/j.rse.2017.12.019.

Lawrence, M.G., Lelieveld, J., 2010. Atmospheric pollutant outflow from southern Asia: A review. Atmos. Chem. Phys. 10, 11017–11096. https://doi.org/10.5194/acp-10-11017-2010.

Lee, H.-H., Bar-Or, R.Z., Wang, C., 2016. Biomass Burning Aerosols and the Low Visibility Events in Southeast Asia. Atmos. Chem. Phys. Discuss. 1–55. https://doi.org/10.5194/acp-2016-504.

Levy, R.C., Mattoo, S., Munchak, L.A., Remer, L.A., Sayer, A.M., Patadia, F., Hsu, N.C., 2013. The Collection 6 MODIS aerosol products over land and ocean. Atmos. Meas. Tech. 6, 2989–3034. https://doi.org/10.5194/amt-6-2989-2013.

Levy, R.C., Remer, L. a., Martins, J.V., Kaufman, Y.J., Plana-Fattori, a., Redemann, J., Wenny, B., 2005. Evaluation of the MODIS Aerosol Retrievals over Ocean and Land during CLAMS. J. Atmos. Sci. 62, 974–992. https://doi.org/10.1175/JAS3391.1.

Livingston, J.M., Redemann, J., Shinozuka, Y., Johnson, R., Russell, P.B., Zhang, Q., Mattoo, S., Remer, L., Levy, R., Munchak, L., Ramachandran, S., 2014. Comparison of MODIS 3 km and 10 km resolution aerosol optical depth retrievals over land with airborne sunphotometer measurements during ARCTAS summer 2008. Atmos. Chem. Phys. 14, 2015–2038. https://doi.org/10.5194/acp-14-2015-2014.

Mahata, K.S., Rupakheti, M., Panday, A.K., Bhardwaj, P., Naja, M., Singh, A., Mues, A., Cristofanelli, P., Pudasainee, D., Bonasoni, P., Lawrence, M.G., 2018. Observation and analysis of spatiotemporal characteristics of surface ozone and carbon monoxide at multiple sites in the Kathmandu Valley, Nepal. Atmos. Chem. Phys. 18, 14113–14132. https://doi.org/10.5194/acp-18-14113-2018.

Mhawish, A., Banerjee, T., Broday, D.M., Misra, A., Tripathi, S.N., 2017. Evaluation of MODIS Collection 6 aerosol retrieval algorithms over Indo-Gangetic Plain: Implications of aerosols types and mass loading. Remote Sens. Environ. 201, 297–313. https://doi.org/10.1016/j.rse.2017.09.016.

Molina, L.T., Kolb, C.E., de Foy, B., Lamb, B.K., Brune, W.H., Jimenez, J.L., Molina, M.J., 2007. Air quality in North America's most populous city – overview of MCMA-2003 Campaign. Atmos. Chem. Phys. Discuss. 7, 3113–3177. https://doi.org/10.5194/acpd-7-3113-2007.

Mues, A., Lauer, A., Lupascu, A., Rupakheti, M., Kuik, F., Lawrence, M.G., 2018. WRF and WRF-Chem v3.5.1 simulations of meteorology and black carbon concentrations in the Kathmandu Valley. Geosci. Model Dev. (GMD) 11, 2067–2091. https://doi.org/10.5194/gmd-11-2067-2018.

Panday, A.K., Prinn, R.G., 2009. Diurnal cycle of air pollution in the Kathmandu Valley, Nepal: Observations. J. Geophys. Res. 114, D09305. https://doi.org/10.1029/2008JD009777.

Panday, A.K., Prinn, R.G., Schär, C., 2009. Diurnal cycle of air pollution in the Kathmandu Valley, Nepal: 2. Modeling results. J. Geophys. Res. Atmos. 114. https://doi.org/10.1029/2008JD009808.

Pistone, K., Praveen, P.S., Thomas, R.M., Ramanathan, V., Wilcox, E.M., Bender, F.A.M., 2016. Observed correlations between aerosol and cloud properties in an Indian Ocean trade cumulus regime. Atmos. Chem. Phys. 16, 5203–5227. https://doi.org/10.5194/acp-16-5203-2016.

Putero, D., Cristofanelli, P., Marinoni, A., Adhikary, B., Duchi, R., Shrestha, S.D., Verza, G.P., Landi, T.C., Calzolari, F., Busetto, M., Agrillo, G., Biancofiore, F., Di Carlo, P., Panday, A.K., Rupakheti, M., Bonasoni, P., 2015. Seasonal variation of ozone and black carbon observed at Paknajol, an urban site in the Kathmandu Valley, Nepal. Atmos. Chem. Phys. 15, 13957–13971. https://doi.org/10.5194/acp-15-13957-2015.

Qin, K., Wu, L., Wong, M.S., Letu, H., Hu, M., Lang, H., Sheng, S., Teng, J., Xiao, X., Yuan, L., 2016. Trans-boundary aerosol transport during a winter haze episode in China revealed by ground-based Lidar and CALIPSO satellite. Atmos. Environ. 141, 20–29. https://doi.org/10.1016/j.atmosenv.2016.06.042.

Regmi, R.P., Kitada, T., 2003. Human-air pollution exposure map of the Kathmandu valley, Nepal: Assesment based on chemical transport simulation. J. Global Environ. Eng. 9, 89–109.

Romero, H., Ihl, M., Rivera, A., Zalazar, P., Azocar, P., 1999. Rapid urban growth, land-use changes and air pollution in Santiago, Chile. Atmos. Environ. 33, 4039–4047. https://doi.org/10.1016/S1352-2310(99)00145-4.

Ross, S.M., 2017. Testing Statistical Hypotheses. In: Introductory Statistics. Elsevier, pp. 381–432. https://doi.org/10.1016/B978-0-12-804317-2.00009-6.

Rupakheti, D., Adhikary, B., Praveen, P.S., Rupakheti, M., Kang, S., Mahata, K.S., Naja, M., Zhang, Q., Panday, A.K., Lawrence, M.G., 2017. Pre-monsoon air quality over Lumbini, a world heritage site along the Himalayan foothills. Atmos. Chem. Phys. 17, 11041–11063. https://doi.org/10.5194/acp-17-11041-2017.

Sarkar, C., Sinha, V., Sinha, B., Panday, A.K., Rupakheti, M., Lawrence, M.G., 2017. Source apportionment of NMVOCs in the Kathmandu Valley during the SusKat-ABC international field campaign using positive matrix factorization. Atmos. Chem. Phys. 17, 8129–8156. https://doi.org/10.5194/acp-17-8129-2017.

Saud, T., Gautam, R., Mandal, T.K., Gadi, R., Singh, D.P., Sharma, S.K., Dahiya, M., Saxena, M., 2012. Emission estimates of organic and elemental carbon from household biomass fuel used over the Indo-Gangetic Plain (IGP), India. Atmos. Environ. 61, 212–220. https://doi.org/10.1016/j.atmosenv.2012.07.030.

Seinfeld, J.H., Pandis, S.N., 2006. Atmospheric Chemistry and Physics: From Air Pollution to Climate Change. Atmos. Chem. Phys. https://doi.org/10.1063/1.882420.

Shakya, K.M., Rupakheti, M., Shahi, A., Maskey, R., Pradhan, B., Panday, A., Puppala, S.P., Lawrence, M., Peltier, R.E., 2017. Near-road sampling of PM2:5, BC, and fine-particle chemical components in Kathmandu Valley, Nepal. Atmos. Chem. Phys. 17, 6503–6516. https://doi.org/10.5194/acp-17-6503-2017.

Sharma, R.K., Bhattarai, B.K., Sapkota, B.K., Gewali, M.B., Kjeldstad, B., 2012. Black carbon aerosols variation in Kathmandu valley, Nepal. Atmos. Environ. 63, 282–288. https://doi.org/10.1016/j.atmosenv.2012.09.023.

Sharma, S.K., Mandal, T.K., Srivastava, M.K., Chatterjee, A., Jain, S., Saxena, M., Singh, B.P., Saraswati, Sharma, A., Adak, A.K., Ghosh, S., 2016. Spatio-temporal variation in chemical characteristics of PM10 over Indo Gangetic Plain of India. Environ. Sci. Pollut. Res. 23, 18809–18822. https://doi.org/10.1007/s11356-016-7025-2.

Sharma, U.K., Kajii, Y., Akimoto, H., 2000. Characterization of NMHCs in downtown urban center Kathmandu and rural site Nagarkot in Nepal. Atmos. Environ. 34, 3297–3307. https://doi.org/10.1016/S1352-2310(99)00485-9.

Shrestha, R.M., Rajbhandari, S., 2010. Energy and environmental implications of carbon emission reduction targets: Case of Kathmandu Valley, Nepal. Energy Policy 38, 4818–4827. https://doi.org/10.1016/j.enpol.2009.11.088.

Shrestha, S., Puppala, S.P., Adhikary, B., Shrestha, K.L., Panday, A.K., 2017. Influence of semi-volatile aerosols on physical and optical properties of aerosols in the Kathmandu Valley. Atmos. Chem. Phys. Discuss. 1–33. https://doi.org/10.5194/acp-2017-287.

Shrestha, S.R., Kim Oanh, N.T., Xu, Q., Rupakheti, M., Lawrence, M.G., 2013. Analysis of the vehicle fleet in the Kathmandu Valley for estimation of environment and climate co-benefits of technology intrusions. Atmos. Environ. 81, 579–590. https://doi.org/10.1016/j.atmosenv.2013.09.050.

Skamarock, W., Klemp, J., Dudhia, J., Gill, D., Barker, D., 2008. A description of the Advanced Research WRF version 3, Technical Report NCAR/TN475 + STR. Boulder, Colorado. https://doi.org/10.5065/D68S4MVH.

Stockwell, C.E., Christian, T.J., Goetz, J.D., Jayarathne, T., Bhave, P.V., Praveen, P.S., Adhikari, S., Maharjan, R., DeCarlo, P.F., Stone, E.A., Saikawa, E., Blake, D.R., Simpson, I.J., Yokelson, R.J., Panday, A.K., 2016. Nepal Ambient Monitoring and Source Testing Experiment (NAMaSTE): emissions of trace gases and light-absorbing carbon from wood and dung cooking fires, garbage and crop residue burning, brick kilns, and other sources. Atmos. Chem. Phys. 16, 11043–11081. https://doi.org/10.5194/acp-16-11043-2016.

Stone, E.A., Schauer, J.J., Pradhan, B.B., Dangol, P.M., Habib, G., Venkataraman, C., Ramanathan, V., 2010. Characterization of emissions from South Asian biofuels and application to source apportionment of carbonaceous aerosol in the Himalayas. J. Geophys. Res. Atmos. 115, 1–14. https://doi.org/10.1029/2009JD011881.

Tiwari, S., 2013. Variability of Aerosol Parameters Derived from Ground and Satellite Measurements over Varanasi Located in the Indo-Gangetic Basin. Aerosol Air Qual. Res. 13, 627–638. https://doi.org/10.4209/aaqr.2012.06.0162.

van Vuuren, D.P., den Elzen, M.G.J., Lucas, P.L., Eickhout, B., Strengers, B.J., van Ruijven, B., Wonink, S., van Houdt, R., 2007. Stabilizing greenhouse gas concentrations at low levels: an assessment of reduction strategies and costs. Climatic Change 81, 119–159. https://doi.org/10.1007/s10584-006-9172-9.

van Vuuren, D.P., Edmonds, J.A., Kainuma, M., Riahi, K., Weyant, J., 2011. A special issue on the RCPs. Climatic Change 109, 1–4. https://doi.org/10.1007/s10584-011-0157-y.

Vinoj, V., Anjan, A., Sudhakar, M., Satheesh, S.K., Srinivasan, J., Moorthy, K.K., 2007. Latitudinal variation of aerosol optical depths from northern Arabian Sea to Antarctica. Geophys. Res. Lett. 34, L10807. https://doi.org/10.1029/2007GL029419.

Zhong, M., Saikawa, E., Avramov, A., Chen, C., Sun, B., Ye, W., Keene, W.C., Yokelson, R.J., Jayarathne, T., Stone, E.A., Rupakheti, M., Panday, A.K., 2018. Nepal Ambient Monitoring and Source Testing Experiment (NAMaSTE): Emissions of particulate matter and sulfur dioxide from vehicles and brick kilns and their impacts on air quality in the Kathmandu Valley, Nepal. Atmos. Chem. Phys. Discuss. 1–34. https://doi.org/10.5194/acp-2018-599.

Web reference

http://worldpopulationreview.com/world-cities/kathmandu-population/ last assessed on 2nd March, 2018.